Journal of
Plant Development Sciences
Meerut, India

RESEARCH ARTICLE

BIOGENIC SYNTHESIS AND CHARACTERIZATION OF NANO-HYDROXYAPATITE USING *BACILLUS SUBTILIS*, *BACILLUS LICHENIFORMIS*, AND *PSEUDOMONAS FLUORESCENS*

Akhilesh Kumar Dwivedi, Ashwani Kumar* and Sachin Kumar

Department of Biotechnology, KVSCOS, Swami Vivekanand Subharti University, Meerut, India
Department of Bioinformatics, Janta Vedic College, Baraut, Baghpat, -250611, India
Email: amritdhra1981@gmail.com

Received-28.05.2025, Revised-12.06.2025, Accepted-26.06.2025

Abstract: This study investigates the biogenic synthesis of nano-hydroxyapatite (nHAP) using *Bacillus licheniformis*, *Bacillus subtilis*, and *Pseudomonas fluorescens*, followed by comprehensive characterization to assess their physicochemical and structural properties. UV–Vis spectroscopy confirmed nanoparticle formation with absorption peaks at 238 and 280 nm (*B. licheniformis*), 241 and 278 nm (*B. subtilis*), and 245 and 281 nm (*P. fluorescens*), suggesting nucleation and presence of organic moieties. Spectral shoulders in *B. subtilis* and *P. fluorescens* indicated biomolecular interaction, unlike the sharper profile of *B. licheniformis*. FTIR analysis showed characteristic phosphate (PO_4^{3-}) bands (~1040 and 560–565 cm^{-1}), hydroxyl groups (~3570 cm^{-1}), and minor carbonate (~1450 cm^{-1}) in all samples. Strong amide I (~1640 cm^{-1}) and II (~1540 cm^{-1}) bands in *B. subtilis* and *P. fluorescens* pointed to proteinaceous capping and biogenic origin, whereas *B. licheniformis* had sharper phosphate peaks and minimal organic signatures, indicating higher crystallinity. EDX confirmed elemental composition with Ca/P ratios near the ideal 1.67. *B. licheniformis* (1.61) produced the most stoichiometric and pure nHAP, followed by *B. subtilis* (1.59) and *P. fluorescens* (1.58), aligning with FTIR observations. DLS and zeta potential results showed *B. licheniformis* synthesized the smallest (32.4 ± 1.2 nm), most monodisperse (PDI 0.186), and stable (−34.2 ± 1.7 mV) particles. In contrast, *P. fluorescens*-derived nHAP was larger (39.3 ± 1.9 nm), more polydisperse (PDI 0.264), and less stable (−26.5 ± 2.2 mV).In conclusion, all three strains synthesized nHAP, but only *B. subtilis* and *P. fluorescens* exhibited strong biogenic characteristics. *B. licheniformis* yielded highly crystalline, near-stoichiometric nHAP, resembling chemically synthesized material, making it ideal for high-purity applications such as agriculture.

Keywords: Agricultural nanomaterials, *Bacillus licheniformis*, *Bacillus subtilis*, *Pseudomonas fluorescens*

INTRODUCTION

Phosphorus (P) is a vital macronutrient required for various physiological and biochemical processes in plants, including photosynthesis, energy transfer, signal transduction, and macromolecular biosynthesis. Despite its importance, phosphorus is one of the least mobile and most limiting nutrients in many agricultural soils due to its strong fixation with iron, aluminum, and calcium compounds. Consequently, phosphate fertilizers are extensively used to meet crop demands. However, conventional phosphorus fertilizers, such as superphosphate and diammonium phosphate, are often inefficient—only 10–25% of applied phosphorus is absorbed by plants, with the remainder contributing to environmental issues such as eutrophication and groundwater contamination (Jupp *et al*., 2021).

In recent years, nano-hydroxyapatite ($Ca_{10}(PO_4)_6(OH)_2$) has attracted considerable interest as a sustainable and efficient phosphorus fertilizer. Its nanoscale dimension increases surface area and solubility, allowing for controlled and targeted nutrient release. Studies have shown that nHAP can serve as a slow-release phosphorus source, enhancing nutrient use efficiency while reducing the risk of leaching and runoff in agricultural systems (Noruzi *et al*., 2023). Furthermore, nano-HA may also improve soil structure and interact positively with soil microbiota, contributing to long-term soil health.

Despite its advantages, traditional chemical synthesis methods for nHAP are often energy-intensive, expensive, and involve hazardous chemicals. To address these limitations, biogenic synthesis, also known as microbial synthesis, is being explored as a green and sustainable alternative. Certain microorganisms, especially phosphate-solubilizing bacteria (PSB), can biologically precipitate calcium phosphate nanoparticles under ambient conditions through metabolic processes involving the production of organic acids, phosphatases, and exopolysaccharides. These natural metabolites create a localized environment that favors nucleation and growth of hydroxyapatite crystals (Fishman *et al*., 2018).

*Corresponding Author

Among these microbes, *Bacillus subtilis*, *Bacillus licheniformis*, and *Pseudomonas fluorescens* are especially noteworthy. These strains are widely recognized as plant growth-promoting rhizobacteria (PGPR), with well-documented capabilities in phosphorus solubilization, nitrogen fixation, production of indole-3-acetic acid (IAA), and biological control of pathogens. Moreover, these microbes thrive in diverse soil environments and have been effectively used in biofertilizer formulations (Ng *et al*., 2022). Their use in synthesizing nHAP offers a dual advantage—enhancing nutrient availability through nanotechnology while also improving soil microbial health and crop resilience.

Incorporating biogenically synthesized nHAP into agricultural practices offers a unique intersection of biotechnology and sustainable farming. Compared to chemically synthesized counterparts, bio-nHAP may possess surface-bound biomolecules that improve biocompatibility and interaction with soil-root systems. However, detailed comparative studies on the synthesis efficiency and nanoparticle characteristics among different PGPR strains are limited.

This study explores the biogenic synthesis of nHAp using three agriculturally relevant bacterial strain *i.e.*, *Bacillus subtilis*, *Bacillus licheniformis*, and *Pseudomonas fluorescens* and evaluates their efficiency in producing nanoparticles. The synthesized nHAP particles were subjected to comprehensive physicochemical characterization using XRD, SEM, FTIR, and zeta potential analysis to know their physicochemical properties. Understanding these properties is crucial, as they influence the nanoparticles' solubility, bioavailability, and interaction with soil and plant systems. The findings could pave the way for scalable, eco-friendly nanomaterial-based solutions to address global challenges in food security and environmental sustainability.

MATERIALS AND METHODS

Chemicals and Reagents

All chemicals used in this study were of analytical grade and used without further purification. Calcium chloride dihydrate ($CaCl_2 \cdot 2H_2O$) and Di-Pottasium Hydrogen Phosphate (K_2HPO_4), required for hydroxyapatite synthesis, were purchased from Sigma-Aldrich. Sodium hydroxide (NaOH), ethanol, and nutrient broth components were procured from HiMedia Laboratories (India). Double distilled deionized water was used throughout the experiments to ensure purity and prevent contamination.

Microorganism Selection and Cultivation

Pure cultures of *Bacillus subtilis* (MTCC 1305), *Bacillus licheniformis* (MTCC 3212),were obtained from the Microbial Type Culture Collection (MTCC), Institute of Microbial Technology (IMTECH), Chandigarh, and *Pseudomonas fluorescence* (IIHR-PF-2) from India and Indian institute of Horticulture Research.

Each bacterial strain was revived in sterile nutrient broth and incubated at 37°C for 24 hours under shaking conditions (120 rpm) to ensure proper aeration and exponential growth. After incubation, the optical density (OD_{600}) of the cultures was monitored to confirm the active growth phase, typically reaching an OD_{600} of 0.8–1.0 before further processing.

Biosynthesis of Nano-Hydroxyapatite (nHAp)

In this investigation, nano-hydroxyapatite (nHAP) was biologically synthesized using three bacterial strains: *Bacillus subtilis* (MTCC 1305), *Bacillus licheniformis* (MTCC 3212), and *Pseudomonas fluorescens* (IIHR-PF-2) from India and Indian institute of Horticulture Research. For inoculum preparation, nutrient broth (NB) was sterilized by autoclaving (20 minutes at 15 psi and 121 ± 1 °C). A single colony of each bacterial strain was aseptically introduced into 10 mL of this sterilized medium and incubated for 12 hours at 37 °C with constant shaking at 200 rpm using a shaker incubator (REMI-CIS-18 Pulse).

To initiate the synthesis of nHAP, 1% (v/v) of this preculture was inoculated into 100 mL of fresh NB, supplemented with 3% (w/v) K_2HPO_4. This whole process was conducted in three separate experimental replicates, each incubated under identical conditions (37 °C, 200 rpm) for 24 hours. Following incubation, the cultures were centrifuged at 10,000 rpm and 25 °C for 15 minutes (Eppendorf 5804 R, Rotor F-34-6-38). The resulting supernatants were carefully collected for phosphate analysis. Subsequently, $CaCl_2$ was added to each supernatant to achieve a final calcium-to-phosphorus (Ca/P) molar ratio of 5:3.

The resulting mixtures were incubated once more under the same conditions (37 °C, 200 rpm for 24 hours), after which a second centrifugation step was carried out under identical parameters to recover the precipitates. These pellets were washed three times with double-distilled water and air-dried. The dried material was then sterilized via autoclaving (20 minutes, 15 psi, 121 ± 1 °C), followed by calcination at 500 °C for 6 hours in a muffle furnace (SHI-205, Shivam Instruments, Delhi, India), using a heating rate of 10 °C per minute. The final product was collected and stored for subsequent characterization.

Characterization of Synthesized nHAP

The synthesized nano-hydroxyapatite (nHAp) was subjected to detailed physicochemical characterization using the following methods:

UV–Visible Spectroscopy: The optical properties and initial confirmation of nanoparticle formation were evaluated using a UV-Vis spectrophotometer (Shimadzu, UV-VIS, 1900i). The absorbance spectra were recorded in the range of 200–400 nm.

Fourier Transform Infrared Spectroscopy (FTIR): FTIR analysis was performed using a Jasco FTIR-4X FTIR Spectrometer in the range of 400–4000 cm^{-1}. The presence of functional groups such as phosphate (PO_4^{3-}), hydroxyl (OH^-) and carbonate (CO_3^{2-}) was identified to confirm the formation of hydroxyapatite.

Energy-Dispersive X-ray Spectroscopy (EDX): Elemental composition of the nanoparticles was determined using EDX (Oxford Instruments X-act) attached to the SEM instrument (ZEISS EVO 18). Peaks corresponding to calcium (Ca), phosphorus (P), and oxygen (O) confirmed the purity of hydroxyapatite.

Dynamic Light Scattering (DLS) and Zeta Potential Analysis: Particle size distribution and surface charge of the synthesized nHAp were measured using a Zeta Sizer Nano ZS (Malvern Instruments). DLS provided the average hydrodynamic diameter of the nanoparticles, while zeta potential analysis assessed the surface charge, indicating the stability of the nanoparticle suspension.

Statistical Analysis

All experiments were performed in triplicate. The mean values and standard deviations were calculated using Microsoft Excel. Where applicable, statistical significance between groups was determined using one-way ANOVA, with $p< 0.05$ considered statistically significant.

RESULTS AND DISCUSSION

Synthesis and UV–Visible Spectroscopic Analysis of nHAp

The biosynthesis of nano-hydroxyapatite (nHAp) was successfully achieved using *Bacillus licheniformis*, *Bacillus subtilis*, and *Pseudomonas fluorescens*. The formation of a white precipitate in the bacterial culture supernatants after incubation indicated successful nanoparticle synthesis. To confirm and monitor this process, UV–Visible spectrophotometry was performed.

The UV–Visible spectroscopic analysis of nano-hydroxyapatite (nHAP) synthesized using *Bacillus licheniformis*, *Bacillus subtilis* and *Pseudomonas fluorescens* revealed distinct absorbance patterns, reflecting differences in nanoparticle formation across the bacterial strains (Fig. 1). All three samples showed a strong peak between 230 and 250 nm, confirming the presence of phosphate groups and the successful formation of hydroxyapatite (Abraham *et al*., 2024).

Among the three, the nHAP synthesized by *Bacillus licheniformis* showed the highest absorbance intensity with a sharp peak near 240 nm, suggesting the formation of smaller, well-dispersed, and highly crystalline nanoparticles (Silva-Holguín et al., 2020). Additionally, a weak shoulder peak around 280 nm was observed, possibly due to the presence of organic residues associated with the particles as capping agents that naturally stabilize the nanoparticles (Podila *et al*., 2012).

In contrast, the nHAP produced by *Bacillus subtilis* exhibited a slightly red-shifted peak around 245 nm with moderate absorbance intensity. This may be indicative of slightly larger particle size or lower crystallinity compared to those formed by *B. licheniformis*. Additionally, a weak shoulder peak around 280 nm was observed, possibly due to the presence of bacterial metabolites or protein-based capping agents that naturally stabilize the nanoparticles (Podila *et al*., 2012). Similarly, the nHAP synthesized using *Pseudomonas fluorescens* displayed the weaker absorbance intensity with the main peak appearing near 250 nm and a more pronounced shoulder peak around 280 nm. This suggests the formation of relatively larger or less crystalline particles and greater involvement of organic compounds. The broader peak profile also points to a wider size distribution, which is consistent with higher polydispersity values obtained from Zeta sizer measurements.

Overall, the UV–Vis spectra confirm the successful biosynthesis of nano-hydroxyapatite by all three bacterial strains.

FTIR Spectral Analysis

Fourier Transform Infrared Spectroscopy (FTIR) was employed to confirm the functional groups and assess the structural features of the nano-hydroxyapatite (nHAP) synthesized using *Bacillus licheniformis, Bacillus subtilis,* and *Pseudomonas fluorescens*. The spectra of all three samples revealed characteristic phosphate and hydroxyl vibrations confirming successful formation of hydroxyapatite, with variations reflecting differences in crystallinity and organic content (Fig. 2).

The nHAP synthesized by Bacillus licheniformis exhibited sharp and strong phosphate peaks at 1045 cm^{-1} (asymmetric stretching) and 565 cm^{-1} (bending vibration), which are typical of well-crystallized hydroxyapatite (Rey *et al*., 1991; Termíne& Posner, 1966). A weak but distinct O–H stretching band around ~3570 cm^{-1} confirmed the presence of structural hydroxyl groups within the apatite lattice (Koutsopoulos, 2002). A minor band near ~1450 cm^{-1} was attributed to H–O–H bending or traces of carbonate, possibly due to atmospheric CO_2 adsorption. A minor band near ~1540 cm^{-1} was attributed to N–H amide bands suggested interaction from biological residues.

In comparison, the FTIR spectrum of *Bacillus subtilis*-mediated nHAP showed a slightly broadened phosphate stretching band at 1041 cm^{-1} and bending mode at 560 cm^{-1}, suggesting a degree of lattice disorder and reduced crystallinity (Copete, *et al*., 2024). The O–H band at ~3570 cm^{-1} was more prominent, confirming hydroxyl group incorporation. Importantly, an additional absorption near ~1640 cm^{-1}, corresponding to Amide I vibrations (C=O

stretching of peptide bonds), indicated the presence of residual proteins or capping agents from bacterial origin (Socrates, 2004; Paramasivan *et al*., 2023a). This was further supported by slightly distorted phosphate peaks and a weak carbonate-related band near ~1450 cm^{-1}.

The FTIR spectrum of nHAP synthesized using *Pseudomonas fluorescens* showed broader and less intense peaks for phosphate stretching (1030 cm^{-1}) and bending (560 cm^{-1}), consistent with low crystallinity. A moderately intense O–H stretch at ~3565 cm^{-1} confirmed hydroxyl group presence. Stronger Amide I and II bands near 1638 cm^{-1} were clearly observed, indicating significant organic or bacterial residue, commonly seen in biogenic apatite (Gheisari *et al*., 2015; Rey *et al*., 1991). Furthermore, a distinct peak at 874 cm^{-1} was assigned to type B carbonate substitution (CO_3^{2-} replacing PO_4^{3-}), which is often characteristic of biologically derived apatite (Fleet, 2009). Minimal bending around ~1450 cm^{-1} further confirmed weak adsorbed water or carbonate presence.

In summary (Table 1), FTIR analysis confirmed the formation of hydroxyapatite in all three samples. *Bacillus licheniformis* produced the most crystalline and pure form, while *Bacillus subtilis* and *Pseudomonas fluorescens* showed increasing degrees of organic association and carbonate substitution, characteristic of biomimetic synthesis routes.

Energy-Dispersive X-ray Spectroscopy (EDX) Analysis

The elemental composition of the synthesized nano-hydroxyapatite (nHAP) was determined using Energy-Dispersive X-ray Spectroscopy (EDX) to confirm the presence of key elements involved in hydroxyapatite structure. All three samples—synthesized using *Bacillus licheniformis, Bacillus subtilis* and *Pseudomonas fluorescens*—showed strong characteristic peaks corresponding to calcium (Ca), phosphorus (P), and oxygen (O) which are the primary components of hydroxyapatite ($Ca_{10}(PO_4)_6(OH)_2$) (Dorozhkin, 2010; Kokubo &Takadama, 2006).

Among the three (Table 2), the EDX spectrum of the nHAP synthesized by Bacillus licheniformis displayed well-defined and intense peaks for Ca and P, with a Ca/P atomic ratio of 1.61 close to the ideal value of 1.67. This ratio is widely accepted as indicative of high purity which correlates with enhanced crystallinity and bioactivity (Hou *et al*., 2022). This observation aligns with the UV–Vis results showing a sharp peak near 240 nm, suggesting highly crystalline and well-formed particles (Ganta *et al*., 2022). The observed near 280 nm, possibly belongs to capping agent *i.e*.., bacterial proteins or other organic stabilizers (Paramasivan *et al*., 2023b).

In the case of Bacillus subtilis-mediated nHAP, the EDX spectrum revealed the presence of Ca, P, and O, but with slightly broader peaks and a marginally lower Ca/P ratio than the B. licheniformis sample. Deviations from the ideal Ca/P ratio often indicate partial substitution or defects, which can reduce crystallinity and alter biological performance (Ramesh *et al*., 2007). This corresponds with the red-shifted UV peak around 245 nm and the observed shoulder near 280 nm, possibly due to capping by bacterial proteins or other organic stabilizers that slightly alter the elemental purity or structure (Alorku *et al*., 2020).

For the nHAP synthesized by *Pseudomonas fluorescens*, the EDX spectra showed relatively lower intensity peaks and a Ca/P ratio deviating further from the stoichiometric value, indicating either non-stoichiometric HAP formation or the presence of additional elements, likely from extracellular polymeric substances or bacterial metabolites (Priyam *et al*., 2019). This is consistent with the lower absorbance and broader shoulder peak in the UV–Vis spectrum near 280 nm, suggesting lower crystallinity and greater organic association (Viju *et al*., 2018).

These EDX findings further validate the UV–Vis spectral analysis, demonstrating that the bacterial strain used significantly influences the elemental composition, crystallinity, and purity of the resulting nHAP nanoparticles (Paramasivan *et al*., 2023a; Ramesh *et al*., 2007).

Dynamic Light Scattering (DLS) and Zeta Potential Analysis

The particle size distribution and surface charge of nano-hydroxyapatite (nHAp) synthesized using different bacterial strains were evaluated using Dynamic Light Scattering (DLS) and zeta potential analysis (Table 3). The Z-average particle size of nHAp varied depending on the bacterial strain used. *Bacillus licheniformis*-mediated synthesis resulted in the smallest average particle size of 32.4 ± 1.2 nm, followed by *Bacillus subtilis* (35.7 ± 1.6 nm), and *Pseudomonas fluorescens* (39.3 ± 1.9 nm).

The Polydispersity Index (PDI) values for all samples were below 0.3, indicating a narrow and uniform size distribution. Specifically, the PDI values were 0.186 ± 0.010 for *B. subtilis*, 0.221 ± 0.014 for *B. licheniformis*, and 0.264 ± 0.017 for *P. fluorescens*, reflecting good nanoparticle homogeneity (Eltarahony *et al*., 2018).

The zeta potential measurements showed that all the synthesized nanoparticles carried a negative surface charge, which is critical for colloidal stability. The zeta potential values were −34.2 ± 1.7 mV for *B. subtilis*-derived nHAp, −30.8 ± 1.9 mV for *B. licheniformis*, and −26.5 ± 2.2 mV for *P. fluorescens*. These values suggest that the nanoparticles possessed good electrostatic stability in suspension, with *B. subtilis*-derived particles showing the highest stability (Sahba *et al*., 2018).

Table 1. Functional groups represented by the corresponding wavenumbers and interpretations regarding properties of nHAP

Microbial Strain	Wavenumber (cm^{-1})	Functional Group / Vibration	Interpretation
Bacillus licheniformis	~3570	O–H stretching (from hydroxyl in HAP)	Weak but present; confirms hydroxyapatite structure
	1045	PO_4^{3-} asymmetric and symmetric stretching	Sharp and strong; indicates well-formed phosphate groups
	565	PO_4^{3-} bending vibrations	Clear, sharp peaks; high crystallinity
	~1450	H–O–H bending / weak carbonate trace	Very minimal – could be adsorbed water or atmospheric CO_2
	~1540	Amide II bands (N-H banding)	Confirms biological or protein-based interaction
Bacillus subtilis	~3570 (weak)	O–H stretching	Slightly more intense; confirms hydroxyl group in structure
	1041	PO_4^{3-} asymmetric and symmetric stretching	Slightly broadened; mild structural disorder
	~1450	H–O–H bending / weak carbonate trace	Very minimal – could be adsorbed water or atmospheric CO_2
	560	PO_4^{3-} bending vibrations	Present but less sharp than B. licheniformis
	~1640	Amide I bands (protein residues)	Indicate presence of organic capping agents
Pseudomonas fluorescens	~3565	O–H stretching	Moderate intensity; confirms hydroxyl presence
	1030	PO_4^{3-} asymmetric and symmetric stretching	Broadened and less intense; lower crystallinity
	560	PO_4^{3-} bending vibrations	Present but broader compared to other samples
	1638	Amide I and II bands	Stronger bands; clear indication of organic/bacterial residues
	874	CO_3^{2-} substitution bands	Clear carbonate substitution likely due to biogenic synthesis route
	~1450	H–O–H bending / weak carbonate trace	Very minimal – could be adsorbed water or atmospheric CO_2

Table 2. EDX Elemental Composition of Synthesized nHAP Samples

Microbial Strain	Element	Atomic %	Remarks
Bacillus licheniformis	Ca	39.4%	Strong, sharp peak; high intensity
	P	23.3%	Strong, sharp peak
	O	36.2%	Consistent with hydroxyapatite formula
	Others	Traces (>2%)	indicates negligible structural deviation
	Ca/P ratio	**1.61**	Near ideal stoichiometric ratio; suggests high purity and crystallinity
Bacillus subtilis	Ca	38.1%	Moderate peak; slightly broader

	P	24.5%	Moderate peak
	O	35.2%	Within expected range
	Others	Trace (<2%)	Possible organic residues (e.g., C, N)
	Ca/P ratio	**1.59**	indicates minor structural deviation
Pseudomonas fluorescens	Ca	36.4%	Peaks less intense; broader
	P	23.1%	Slightly lower intensity
	O	37.8%	Typical of hydroxyapatite
	Others	Minor (<3%)	Trace of organic/stabilizing components
	Ca/P ratio	**1.58**	Slightly off ideal; moderate purity and crystallinity

Table 3. Zetasizer Analysis of Nano-Hydroxyapatite Synthesized Using Different Bacterial Strains (Mean ± SD, n = 3)

Bacterial Strain	**Z-Average Particle Size (nm)**	**Polydispersity Index (PDI)**	**Zeta Potential (mV)**
Bacillus licheniformis	32.4 ± 1.2	0.186 ± 0.010	−34.2 ± 1.7
Bacillus subtilis	35.7 ± 1.6	0.221 ± 0.014	−30.8 ± 1.9
Pseudomonas fluorescence	39.3 ± 1.9	0.264 ± 0.017	−26.5 ± 2.2

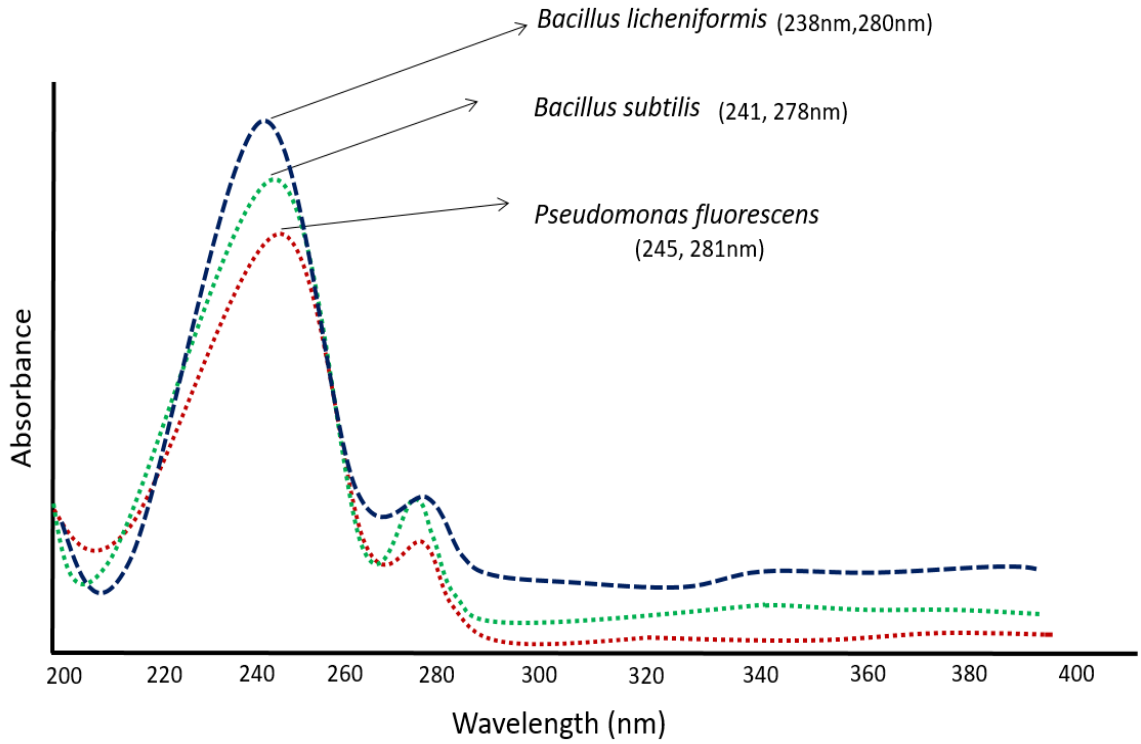

Fig. 1. UV spectrum of nHAP synthesized using different strains

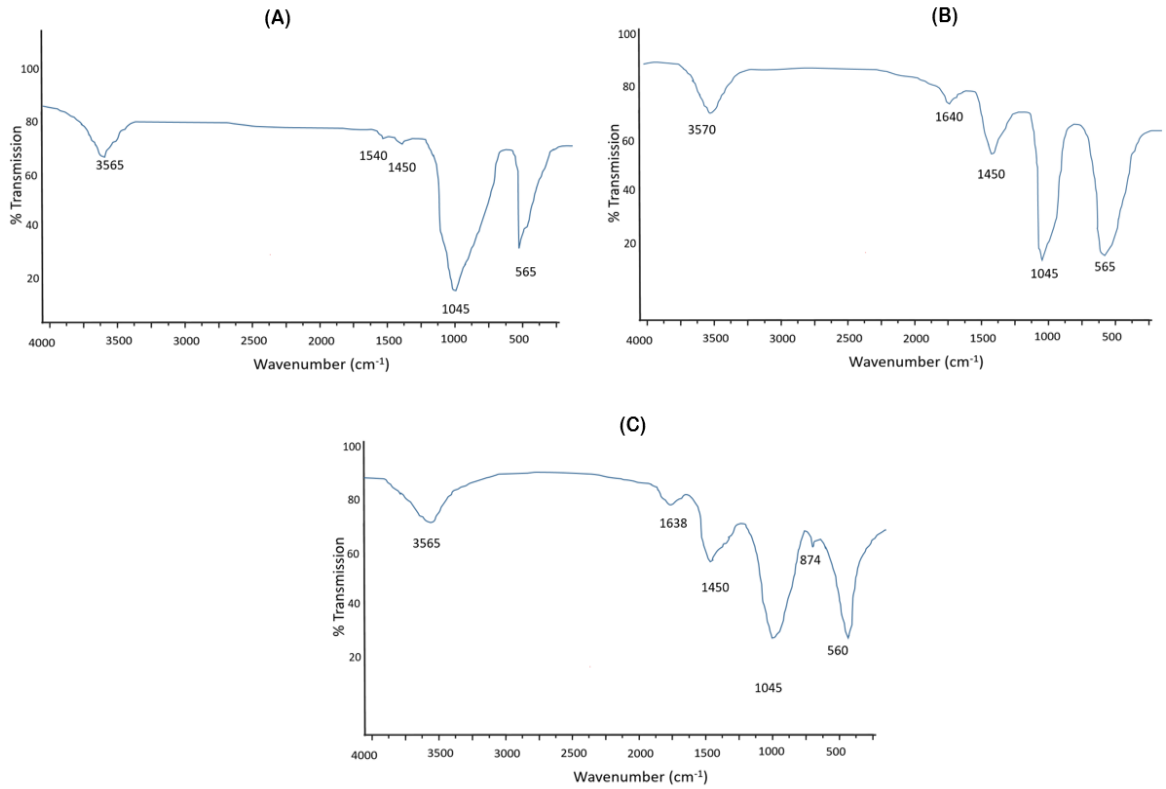

Fig. 2. FTIR Spectrum of nHAP synthesized using different strain (A) *Bacillus licheniformis* (B) *Bacillus subtilis* and (C) *Pseudomonas fluorescens*

CONCLUSION

With notable differences in nanoparticle size, purity, and degree of organic interaction depending on the microbial species used. *Bacillus licheniformis* emerged as the most effective strain in producing stable, well-crystallized nHAP suitable for applications in agriculture, ideal for applications where long-term nutrient supply, structural consistency, and minimal environmental risk are priorities—especially in precision farming or commercial fertilizer formulations.

ACKNOWLEDGEMENT

The authors wish to express their profound gratitude the Swami Vivekananda University, Meerut, Biological R&D center, Insectiscides (India) Limited, Shamli (U.P.), Shriram AgSmart Limited, Kota, and Centre for Advanced Plant Nutrition (CAPN), Ludhiana for their support during data collection. Our profound gratitude also goes to Dr. Ashwani Kumar Department of Biotechnology, KVSCOS, Swami Vivekanand Subharti University, Meerut, India for his guidance and contributions towards this work.

Conflict of interests

The authors declare that there is no competing interest.

REFERENCES

Abraham, A., Sharan Kumar, M., Krishna, D. A. and others. (2024). Development of nano-hydroxyapatite membrane using Momordicacharantia and study of its biodegradability for medical application. *Biomass Conversion and Biorefinery*, **14**, 32289–32301. https://doi.org/10.1007/s13399-023-04929-9.

Google Scholar

Alorku, K., Manoj, M. and Yuan, A. (2020). A plant-mediated synthesis of nanostructured hydroxyapatite for biomedical applications: A review. *RSC Advances*, **10**(67), 40923–40939. https://doi.org/10.1039/D0RA08529D.

Google Scholar

Copete, H., López, E. and Baudin, C. (2024). Synthesis and characterization of B-type carbonated hydroxyapatite materials: Effect of carbonate content on mechanical strength and in vitro degradation. *Boletín de la Sociedad Española de Cerámica y Vidrio*, **63**(4), 255–267. https://doi.org/10.1016/j.bsecv.2023.12.001.

Google Scholar

Dorozhkin, S. V. (2010). Bioceramics of calcium orthophosphates. *Biomaterials*, **31**(7), 1465–1485. https://doi.org/10.1016/j.biomaterials.2009.10.050.

Google Scholar

Eltarahony, M., Zaki, S., ElKady, M. and Abd-El-Haleem, D. (2018). Biosynthesis, characterization of some combined nanoparticles, and its biocide

potency against a broad spectrum of pathogens. *Journal of Nanomaterials*, 2018, Article ID 5263814, 1–13. https://doi.org/10.1155/2018/5263814.

Google Scholar

Fishman, M. R., Giglio, K., Fay, D., *et al.* (2018). Physiological and genetic characterization of calcium phosphate precipitation by Pseudomonas species. *Scientific Reports*, **8**, 10156. https://doi.org/10.1038/s41598-018-28525-4.

Google Scholar

Fleet, M. E. (2009). Infrared spectra of carbonate apatites: ν2-Region bands. *Biomaterials*, **30**(7), 1473–1481. https://doi.org/10.1016/j.biomaterials.2008.12.007.

Google Scholar

Ganta, D. D., Hirpaye, B. Y., Raghavanpillai, S. K. and Menber, S. Y. (2022). Green synthesis of hydroxyapatite nanoparticles using Monoonlongifolium leaf extract for removal of fluoride from aqueous solution. *Journal of Chemistry*, 2022, Article ID 4917604. https://doi.org/10.1155/2022/4917604.

Google Scholar

Gheisari, H., Karamian, E. and Abdellahi, M. (2015). A novel hydroxyapatite–Hardystonite nanocomposite ceramic. *Ceramics International*, **41**(4), 5967–5975. https://doi.org/10.1016/j.ceramint.2015.01.033.

Google Scholar

González-Márquez, H., Peralta-Videa, J. R. and Gardea-Torresdey, J. L. (2018). Physiological and genetic characterization of calcium phosphate precipitation by Pseudomonas species. *Frontiers in Microbiology*, **9**, 2671. https://doi.org/10.3389/fmicb.2018.02671.

Google Scholar

Hou, X., Zhang, L., Zhou, Z., Luo, X., Wang, T., Zhao, X., Lu, B., Chen, F. and Zheng, L. (2022). Calcium phosphate-based biomaterials for bone repair. *Journal of Functional Biomaterials*, **13**(4), 187. https://doi.org/10.3390/jfb13040187.

Google Scholar

Jupp, A. R., Beijer, S., Narain, G. C., Schipper, W. and Slootweg, J. C. (2021). Phosphorus recovery and recycling – closing the loop. *Chemical Society Reviews*, **50**(1), 87–101. https://doi.org/10.1039/d0cs01150a.

Google Scholar

Kokubo, T. and Takadama, H. (2006). How useful is SBF in predicting in vivo bone bioactivity? *Biomaterials*, **27**(15), 2907–2915. https://doi.org/10.1016/j.biomaterials.2006.01.017.

Google Scholar

Koutsopoulos, S. (2002). Synthesis and characterization of hydroxyapatite crystals: A review study on the analytical methods. *Journal of Biomedical Materials Research*, **62**(4), 600–612. https://doi.org/10.1002/jbm.10280.

Google Scholar

Ng, C. W. W., Yan, W. H., Tsim, K. W. K., So, P. S., Xia, Y. T. and To, C. T. (2022). Effects of Bacillus subtilis and Pseudomonas fluorescens as the soil amendment. *Heliyon*, **8**(11), e11674. https://doi.org/10.1016/j.heliyon.2022.e11674.

Google Scholar

Noruzi, M., Hadian, P., Soleimanpour, L., et al. (2023). Hydroxyapatite nanoparticles: an alternative to conventional phosphorus fertilizers in acidic culture media. *Chemical and Biological Technologies in Agriculture*, **10**, 71. https://doi.org/10.1186/s40538-023-00437-0.

Google Scholar

Paramasivan, M., Sampath Kumar, T. S., Kanniyappan, H., Muthuvijayan, V. and Chandra, T. S. (2023a). Biomimetic ion substituted and co-substituted hydroxyapatite nanoparticle synthesis using Serratiamarcescens. *Scientific Reports*, **13**, 4513. https://doi.org/10.1038/s41598-023-30996-z.

Google Scholar

Paramasivan, M., Sampath Kumar, T. S., Kanniyappan, H., Muthuvijayan, V. and Chandra, T. S. (2023b). Microbial biomineralization of hydroxyapatite nanocrystals using Bacillus tequilensis. *Ceramics International*, **49**(4), 5621–5629. https://doi.org/10.1016/j.ceramint.2022.10.138.

Google Scholar

Podila, R., Chen, R., Ke, P. C. and Rao, A. M. (2012). Effects of surface functional groups on the formation of nanoparticle-protein corona. arXiv preprint arXiv:1209.5475. https://arxiv.org/abs/1209.5475.

Google Scholar

Priyam, A., Das, R. K., Schultz, A. and others (2019). A new method for biological synthesis of agriculturally relevant nanohydroxyapatite with elucidated effects on soil bacteria. *Scientific Reports*, **9**, 15083. https://doi.org/10.1038/s41598-019-51514-0.

Google Scholar

Ramesh, S., Tan, C. Y., Hamdi, M., Sopyan, I. and Teng, W. D. (2008). The influence of Ca/P ratio on the properties of hydroxyapatite bioceramics. *Proceedings of SPIE*, 6423, 64233A. https://doi.org/10.1117/12.779890.

Google Scholar

Rey, C., Combes, C., Drouet, C. and Glimcher, M. J. (2009). Bone mineral: Update on chemical composition and structure. *Osteoporosis International*, **20**(6), 1013–1021. https://doi.org/10.1007/s00198-009-0860-y.

Google Scholar

Sahba, R., SeyedSadjadi, M., Sajjadi, A.K., Farhadyar, N. and Sadeghi, B. (2018). Preparation and characterization of friendly colloidal Hydroxyapatite based on natural Milk's casein. *Int. J. Nano Dimens.*, **9** (3): 238-245.

Google Scholar

Silva-Holguín, P. N. and Reyes-López, S. Y. (2020). Synthesis of hydroxyapatite-Ag composite as antimicrobial agent. *Dose-Response*, **18**(3), 1559325820951342. https://doi.org/10.1177/1559325820951342.
Google Scholar

Socrates, G. (2004). Infrared and Raman characteristic group frequencies: Tables and charts (3rd ed.). John Wiley and Sons.
Google Scholar

Terminé, J. D. and Posner, A. S. (1966). Infrared determination of the percentage of crystallinity in apatitic calcium phosphates. *Nature*, **211**(5053), 268–270. https://doi.org/10.1038/211268a0.
Google Scholar

Viju Kumar, V. G. and Ananthu, A. P. (2018). Green synthesis and characterization of iron oxide nanoparticles using *Phyllanthusniruri* extract. *Oriental Journal of Chemistry*, **34**(5), 2473–2479. https://doi.org/10.13005/ojc/340547.
Google Scholar